RSC Advances

PAPER

View Article Online
View Journal | View Issue



Cite this: *RSC Adv.*, 2022, **12**, 18676

# Cellulose derived Pd nano-catalyst for efficient catalysis†

Lingyu Zhang,[a] Siyu Long,[ab] Huibin Jiao,[c] Zhuoyue Liu,[a] Ping Zhang,[a] Aiwen Lei,[b] Wei Gong*[a] and Xianglin Pei *[ab]

Using green, environmentally friendly and resource-rich cellulose as a raw material, a ligand-free and highly dispersed palladium (Pd) nano-catalyst was successfully prepared in a facile way. A variety of characterization results showed that the Pd nanoparticles (NPs) were uniformly spread on the cellulose nanoporous microspheres, with an average particle size of ~2.75 nm. As a carrier, cellulose microspheres with nanoporous structure and rich –OH groups greatly promoted the attachment and distribution of the highly dispersed Pd NPs, along with the diffusion and exchange of reactants, so as to greatly promote the catalytic activity. In the Suzuki–Miyaura coupling reaction, the catalyst of C–Pd exhibited excellent catalytic activity (TOF up to 2126 $h^{-1}$), broad applicability, and good recyclability with almost no active loss in 6 continuous runs. This utilizing of bioresources to build catalyst materials is important for sustainable chemistry.

Received 3rd May 2022
Accepted 16th June 2022

DOI: 10.1039/d2ra02799b

rsc.li/rsc-advances



## 1. Introduction

Under the influence of green chemistry, many chemical processes in organic synthetic chemistry have turned environmentally friendly. For instance, in the field of catalysis, the use of transition metal catalysts to maximize the efficiency of chemical reactions is in line with the background of green chemistry.[1] Generally, homogeneous metal catalysts have better catalytic activity than heterogeneous metal catalysts, based on their utilization of catalytic active sites at a molecular level.[2] However, the separation and purification process of homogeneous metal catalysts are cumbersome and costly.[3] In contrast, the heterogeneous metal catalysts are easy to separate and reusable, and can also highly disperse the nano metals and prevent the agglomeration of the nano metals in the reaction process, thereby effectively catalyzing the reactions.[4] Nowadays, palladium based heterogeneous catalysts have attracted extensive attention due to their excellent catalytic activity and selectivity for building C–C, C–H and C–heteroatom bonds in organic synthesis.[5] However, the strong interaction between Pd–Pd bonds is easy to cause the formation of bulky Pd particles, resulting in the decrease of active catalytic sites and catalytic efficiency.[6] It can be seen that how to highly disperse the Pd NPs is a key factor. As heterogeneous Pd catalysts, the supports can disperse the Pd NPs.[7] Meanwhile, as the attachment site of Pd metals, the support materials can change the interface properties between the support and Pd, and then improve the catalytic performance of the catalyst.[8,9] Therefore, the selection of carrier materials is very important.

Recently, researchers have tried to use various support materials to disperse the metal nano-catalysts. For instance, the metal oxides,[10,11] silica,[12,13] carbon materials,[14,15] metal organic framework (MOFs),[16] covalent organic frameworks (COFs)[17] and so on. Kirlikovali *et al.* obtained a Zr-based catalyst (Zr-MOFs) by loading zirconium metal on metal–organic frameworks, which showed good effects on the hydrolysis and detoxification of nerve agents and mimetics.[18] Kang *et al.* used $SiO_2$ grafted by silane coupling agents as support to synthesis a Pd/AS-$SiO_2$ catalyst, and applied it to Suzuki reaction.[19] Yan *et al.* treated graphene with acid to generate anchoring sites such as hydroxyl and carboxyl groups to prepare atomic layer deposition Pd nano-catalyst for highly selective hydrogenation of 1,3-butadiene.[20] Pagar *et al.* obtained mesoporous carbon materials prepared *via* mesoporous silica by using a templating agent, and then used it as support to prepare Rh-based catalysts to efficiently catalyze the hydroformylation of higher olefins.[21] However, these supported materials may suffer from the problems such as unstable structure, need for further modification (no anchoring metal sites), high synthesis cost, complex synthesis process, non-renewable petrochemical resources. Therefore, it is of great significance to design and synthesize more suitable support materials. Natural biopolymers are rich in resources, renewable, environmentally friendly and stable in structure, which can be used as carrier materials for

[a]School of Materials and Architectural Engineering, Guizhou Normal University, Guiyang 550025, China. E-mail: xianglinpei@163.com; gongw@gznu.edu.cn
[b]College of Chemistry and Molecular Sciences, Wuhan University, Wuhan 430072, China
[c]School of Materials Science and Engineering, Guizhou Minzu University, Guiyang 550025, China

† Electronic supplementary information (ESI) available. See https://doi.org/10.1039/d2ra02799b

heterogeneous catalysts and have gradually become one of the emerging research hotspots in recent years.[22] For example, as the most natural polymer resources in earth, cellulose has gradually attracted the interest of researchers.[23,24] Cellulose-based materials have great advantages as a support for metal catalysts. One aspect is its environmental friendliness, easy availability, and good stability in water and most organic solvents, which is pivotal for a catalyst support[25,26] On the other hand, based on the rigidity of cellulose molecular chains, cellulose with a multilayered nanoporous structure is beneficial for the attachment and dispersion of nano-metals. In addition, cellulose contains a lot of hydroxyl groups, which could serve as metal nucleation centers and provide necessary support for anchoring metal nanoparticles.[27] However, the intermolecular and intramolecular interaction of cellulose is relatively large, and it is difficult to dissolve and melt.[28] Our previous laboratory developed a NaOH/urea aqueous solution to dissolve cellulose, and successfully constructed a nanoporous cellulose microspheres through freeze–thaw technology.[29] The prepared cellulose microspheres have a nanoporous structure, which is conducive to the attachment and dispersion of nanometals, as well as effectively prevent the aggregation of Pd NPs. Based on these considerations, a Pd nano-catalyst supported by cellulose microspheres is highly anticipated.[30]

Herein, we report an effective strategy to synthesize a highly dispersed palladium nano-catalyst immobilized on cellulose. As the support, the nanoporous cellulose microspheres with rich functional groups played vital roles in the formation of tiny Pd NPs. In addition, the prepared catalyst exhibited high catalytic activity in catalyzing the Suzuki–Miyaura coupling reaction, as well as excellent recyclability with no significant active loss after 6 runs. Importantly, this work uses the bioresources as raw materials to construct a cellulose-supported catalyst, which provides a new approach for the application of cellulose-based materials, as well as promotes the implementation of a sustainable society.

## 2. Experimental section

### 2.1 Preparation of the cellulose microspheres

The general preparation procedure for cellulose microspheres was as follows: firstly, 3 g of cellulose powder was dispersed in 100 g of 7 wt% NaOH/12 wt% urea/81 wt% $H_2O$, and a transparent cellulose solution was obtained by vigorous mechanical stirring in the state of half ice and half water. Then, 1.5 mL of epichlorohydrin was added to the above solution and stirred for 30 min under ice bath conditions. Subsequently, after adding 200 g of isooctane and stirring uniformly, 6 g of Span 80 was added to the apparatus. The mixed solution was placed in a 1 L three-necked flask equipped with a mechanical stirrer, and then the above-mentioned cellulose solution was added. The suspension was stirred in an ice bath for 1 h and at room temperature for 3 h to obtain regenerated cellulose nanoporous microspheres. Finally, the microspheres were washed 3 times with deionized water and ethanol respectively, exchanged with *tert*-butanol, and then lyophilized for use.

### 2.2 Preparation of the Pd nano-catalyst supported on cellulose microspheres

The above cellulose microspheres (100 mg), $PdCl_2$ (0.42 mg) and toluene (30 mL) were added to a round-bottomed flask, and then stirred at room temperature for 30 min under a nitrogen atmosphere, then raised the temperature to 85 °C to continue the reaction for 3 h. Afterward, the crude product was filtered, washed and dried to get a palladium nano-catalyst supported on cellulose microspheres.

### 2.3 General procedure for the Suzuki–Miyaura coupling reaction

In a typical experiment, aryl halide (0.5 mmol), arylboronic acid (0.75 mmol), $K_2CO_3$ (1.0 mmol), C–Pd (10 mg) and EtOH/$H_2O$ = 1 : 1 (10 mL) were added to a round-bottomed flask. Then the mixture was magnetically stirred at 85 °C under $N_2$ for certain time to complete the reaction, and the yield of the product was obtained by GC (gas chromatography); for the cycle stability test, the reaction conditions were the same as above, and product formation and the progress of the reaction was monitored by GC.

## 3. Results and discussion

### 3.1 Synthesis and characterization of the C–Pd catalyst

As described in Fig. 1, using renewable resource cellulose as raw materials, a supported Pd nano-catalyst was obtained. Firstly, the cellulose solution dissolved in the NaOH/urea aqueous solution was physically regenerated into cellulose microspheres *via* emulsion method by sol–gel strategy. Then, the cellulose microspheres were impregnated with $PdCl_2$ solution, and the Pd ions were fixed by the hydroxyl groups on the cellulose microspheres. Subsequently, the above mixture was heated to 85 °C in a nitrogen atmosphere, and the Pd ions immobilized on the cellulose were reduced to Pd NPs without the additional reductant to obtain supported the C–Pd catalyst.

In order to investigate the structure of the C–Pd catalyst, a series of characterizations were conducted. Thermal gravimetric analysis (TGA) curves of the blank cellulose and C–Pd depicted in Fig. 2a showed that the 5% weight loss temperatures ($T_{5\%}$) of the blank cellulose and C–Pd were 304.8 °C and 282.5 °C, respectively. When the thermal decomposition temperature was ~800 °C, the weight loss of the sample was about 85%, which was due to the thermal decomposition of the cellulose. TGA data indicated that when the reaction temperature was 85 °C, it would not affect the structure of the support material. Fourier transform infrared spectra (FT-IR) analysis indicated that the characteristic peaks of the blank cellulose at 3428, 2921, 1437, 1378 and 1046 $cm^{-1}$ were defined as O–H stretching vibration, C–H stretching vibration, C–H ribbon vibration, C–H deformation vibration and C–O stretching vibration, respectively (Fig. 2b).[31–33] After loading of Pd particles, those characteristic peaks in blank cellulose also appeared on the C–Pd catalyst, which further indicated that the material preparation temperature of 85 °C would not affect the structure of the cellulose. Scanning electron microscopy (SEM)

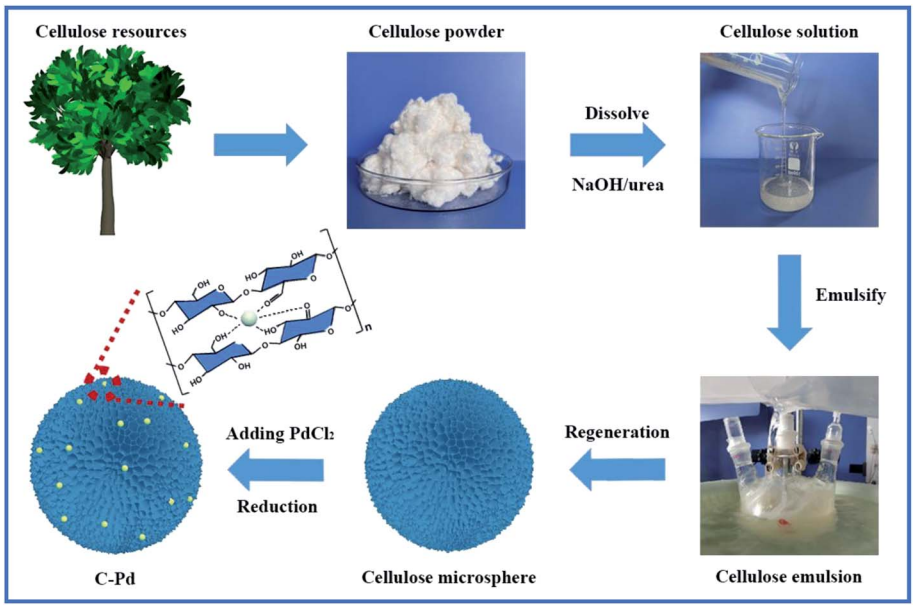


Fig. 1 Schematic illustration for the formation of C–Pd.

represented in Fig. 2c and d revealed that the cellulose microspheres in C–Pd had an unconventional shape, with relatively uniform size and nanoporous structure, which was consistent with the structure of the blank cellulose microspheres (Fig. S1 and S2†). The porous structure of cellulose microspheres was conducive to the adhesion and dispersion of Pd particles, as well the diffusion and exchange of the reactive substances, which was very critical for the support material of the catalyst. Energy dispersive X-ray spectroscopy (EDX) mapping analysis of the C–Pd (Fig. 2e1–e4) proved that the C–Pd catalyst contained elements of C, O and Pd, and the Pd element was evenly dispersed on the carrier, indicating the Pd particles were successfully loaded on the cellulose microspheres. X-ray powder diffraction (XRD) patterns in Fig. 2f showed that the diffraction peaks ascribed to blank cellulose centered at 11.8°, 19.9°, and 21.5° corresponding to the (1 $\bar{1}$0), (110), and (200) reflections of

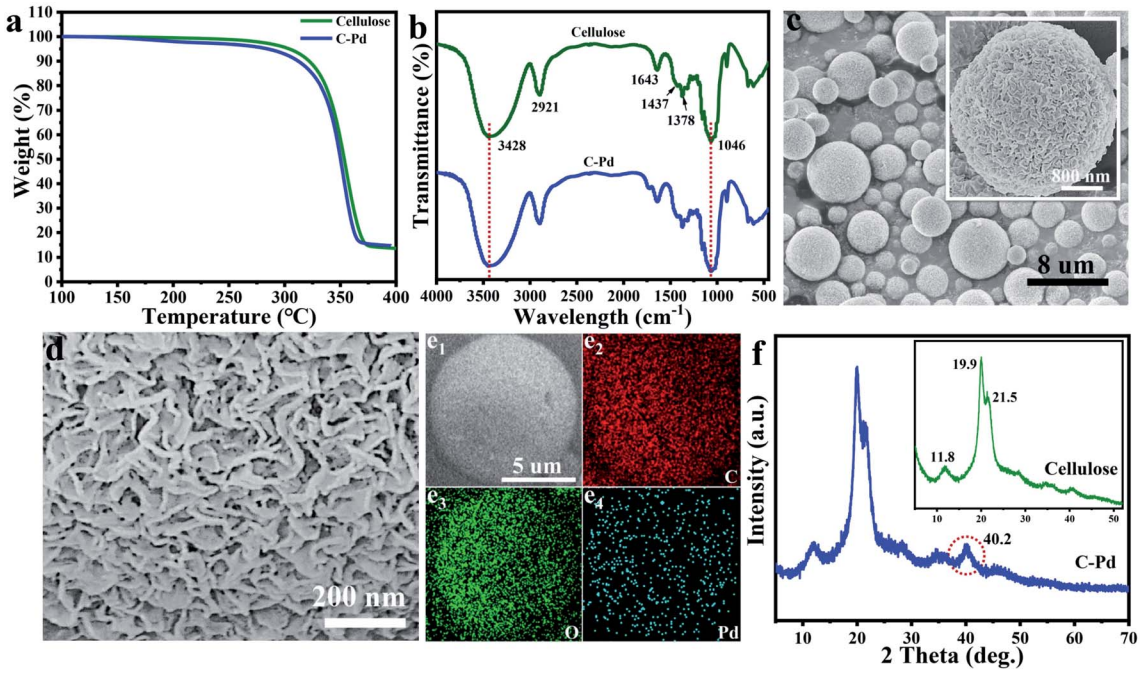


Fig. 2 TGA curves of the blank cellulose and C–Pd (a). FT-IR spectra of the blank cellulose and C–Pd (b). SEM image of C–Pd (c), inset with a single C–Pd microsphere. Partial enlargement of a C–Pd microsphere (d). EDX mapping of C–Pd ($e_1$–$e_4$). XRD patterns of the blank cellulose and C–Pd (f).

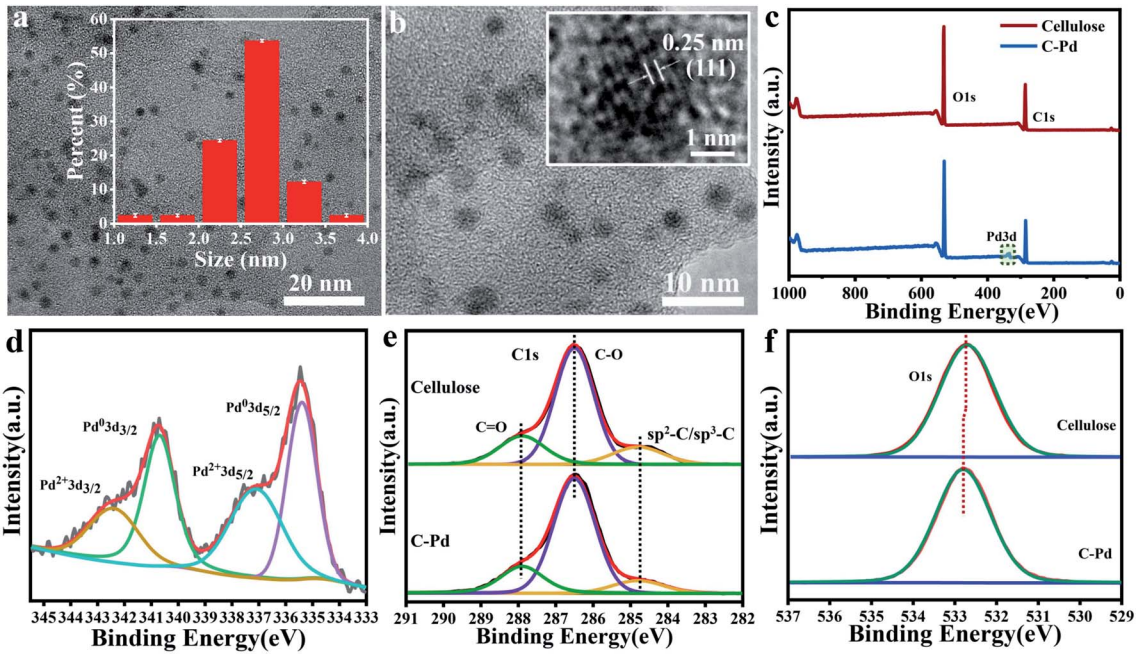


Fig. 3 TEM images of C–Pd (a, b), inset (a) with the particle size distribution of Pd particles and inset (b) with the high-resolution TEM image of C–Pd. Full-scale XPS spectra of blank cellulose and C–Pd (c). XPS of Pd 3d spectra of the C–Pd (d). XPS of C 1s (e) and O 1s (f) spectra of blank cellulose and C–Pd.

cellulose lattice respectively.[34,35] After the introduction of Pd particles, the C–Pd catalyst showed a new characteristic peak at about $2\theta = 40.2$, which corresponded to the (111) reflection of Pd, further indicating the successful loading of Pd particles.[36]

To observe the structure of the Pd NPs immobilized on cellulose, transmission electron microscopy (TEM) was conducted. The results in Fig. 3a and b showed that the Pd particles were spherical and uniformly dispersed on the microspheres without obvious aggregation, with an average particle size of about 2.75 ± 0.4 nm (inset in Fig. 3a). It was not difficult to imagine that these highly dispersed Pd NPs with abundant active sites could greatly promote the chemical reaction. Moreover, a typical high-resolution TEM image (inset in Fig. 3b) also showed a clear lattice fringe with *d*-space of 0.25 nm attributed to the characteristic response of Pd, which further confirmed the existence of Pd.[37] In order to study the surface composition and chemical state of the C–Pd catalyst, X-ray photoelectron spectroscopy (XPS) was conducted. The overall XPS spectrum of the catalyst (Fig. 3c) showed that the C–Pd was composed of three elements: C, O and Pd, which further proved that the Pd NPs were successfully loaded on the cellulose. The Pd 3d spectrum in Fig. 3d showed the binding energy peaks of various core levels of Pd. The binding energies of 340.69 and 335.40 eV were corresponding to $Pd^0$ $3d_{3/2}$ and $Pd^0$ $3d_{5/2}$, while the binding energies of 342.43 eV and 337.13 eV ascribed to $Pd^{2+}$ $3d_{3/2}$ and $Pd^{2+}$ $3d_{5/2}$, which indicated that most of the Pd species in C–Pd presented the characteristics of metallic Pd (0).[38] The interaction between Pd NPs and cellulose matrix was also investigated by XPS, and the spectrum had been calibrated with C 1s of 284.80 eV. As shown in Fig. 3e, the binding energy peaks of C 1s in blank cellulose were mostly concentrated at 284.80 eV, 286.50 eV and 287.94 eV corresponding to the $sp^2$–C/$sp^3$–C, C–O and C=O bonds, respectively.[39] After loading of Pd NPs, the binding energy peaks in C–Pd was basically unchanged, indicating that there was no interaction between C and Pd. While in the O 1s spectrum (Fig. 3f), the binding energy peak of blank cellulose microspheres appeared at 532.70 eV, which shifted to 532.82 eV after the loading of Pd NPs. The shift was likely due to the metal–ligand interaction, and the electrons transferred from the lone pair of O atoms to Pd, leading to a reduction in the electron cloud density of O atoms and an increase in binding energy. These results all indicated that the well-

Table 1 Comparison of catalytic activity of different catalysts[a]

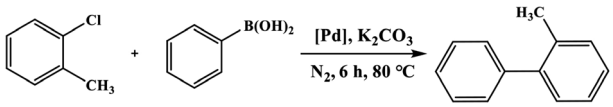


| Entry | Catalyst | Solvent | Yield[b] (%) |
|---|---|---|---|
| 1 | C–Pd | $H_2O$ | 22.5 |
| 2 | C–Pd | EtOH | 63.6 |
| 3 | C–Pd | EtOH : $H_2O$ = 1 : 1 | >99 |
| 4 | Blank cellulose | EtOH : $H_2O$ = 1 : 1 | None |
| 5 | $Pd(OAc)_2$ | EtOH : $H_2O$ = 1 : 1 | 41.1 |
| 6 | Pd/C | EtOH : $H_2O$ = 1 : 1 | 67.5 |
| 7 | Nano-Pd | EtOH : $H_2O$ = 1 : 1 | 4.1 |

[a] Reaction conditions: *o*-chlorotoluene (0.5 mmol), phenylboronic acid (0.75 mmol), $K_2CO_3$ (1.0 mmol), solvent (10 mL), 0.047 mol% C–Pd ([Pd] : substrate, mol%), 80 °C, 6 h. [b] The yields were determined by GC.

Table 2 Suzuki–Miyaura coupling reaction catalyzed C–Pd[a]

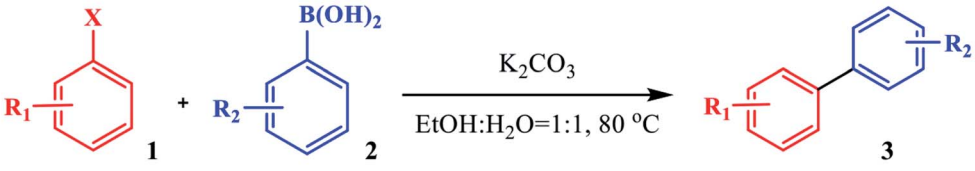


X=I

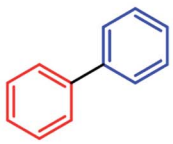

**3a** (>99%, TOF=2126 $h^{-1}$)[b]

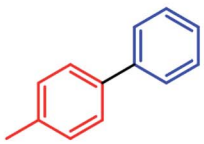

**3b** (>99%, TOF=2126 $h^{-1}$)[b]

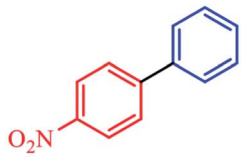


**3c** (>99%, TOF=2126 $h^{-1}$)[b]

X=Br

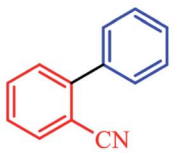


**3d** (>99%, TOF=354 $h^{-1}$)

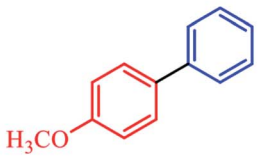


**3e** (>99%, TOF=354 $h^{-1}$)

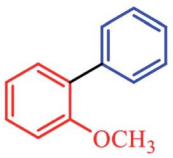


**3f** (93.9%, TOF=333 $h^{-1}$)

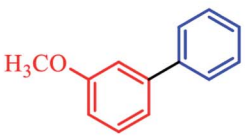


**3g** (74.9%, TOF=266 $h^{-1}$)

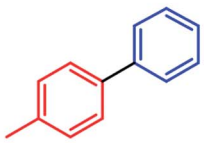

**3h** (92.1%, TOF=327 $h^{-1}$)

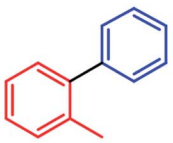

**3i** (87.8%, TOF=311 $h^{-1}$)

X=Cl

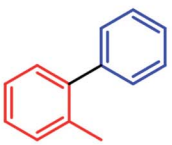

**3j** (>99%, TOF=354 $h^{-1}$)

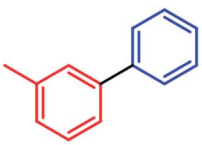

**3k** (69.4%, TOF=246 $h^{-1}$)

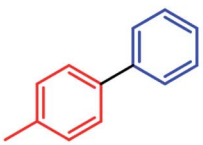

**3l** (90.3%, TOF=320 $h^{-1}$)

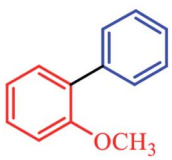


**3m** (93.6%, TOF=332 $h^{-1}$)

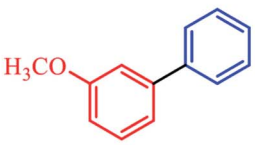


**3n** (72.2%, TOF=256 $h^{-1}$)

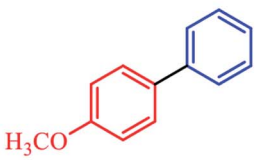


**3o** (99.3%, TOF=352 $h^{-1}$)

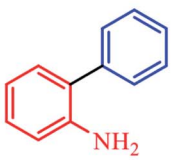


**3p** (>99%, TOF=354 $h^{-1}$)

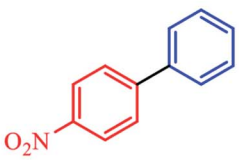


**3q** (>99%, TOF=354 $h^{-1}$)

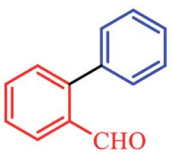


**3r** (>99%, TOF=354 $h^{-1}$)

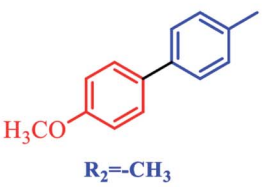


$R_2$=-$CH_3$

**3s** (84.7%, TOF=150 $h^{-1}$)[c]

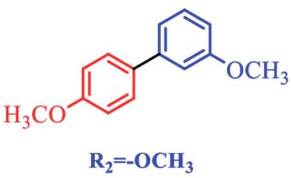


$R_2$=-$OCH_3$

**3t** (83.2%, TOF=148 $h^{-1}$)[c]

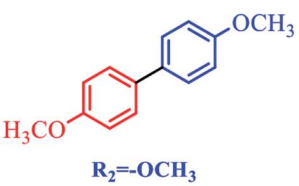


$R_2$=-$OCH_3$

**3u** (80.5%, TOF=143 $h^{-1}$)[c]

[a] Reaction conditions: aryl halides (0.5 mmol), arylboronic acid (0.75 mmol), $K_2CO_3$ (1.0 mmol), 0.047 mol% C–Pd ([Pd] : substrate, mol%), EtOH : $H_2O$ = 1 : 1 (10 mL) at 80 °C for 6 h, and the yields were isolated yields. [b] Reactions were carried out at 80 °C for 1 h. [c] Reactions were carried out at 80 °C for 12 h.

dispersed and firmly immobilized Pd NPs were successfully supported on cellulose. It was conceivable that the well-dispersed C–Pd catalyst with more catalytic active sites could greatly facilitate the progress of chemical reactions.

### 3.2 Catalytic activity of the C–Pd catalyst

As the products of Suzuki–Miyaura coupling reaction could be applied to the synthesis of many pharmaceutical intermediates, natural products, organic materials, *etc.*, which motivated us to use the synthetic C–Pd catalyst to catalyze Suzuki–Miyaura coupling reaction. All the results were compiled in Table 1, by using *o*-chlorotoluene and phenylboronic acid as the model substrates, we first attempted the most commonly used solvent of ethanol and $H_2O$ reported in the literature. It could be seen that the product yield was very low in both solvent ethanol and $H_2O$, but the reaction yield could reach 99% in the mixed solvent of ethanol and $H_2O$. Further, we also used the commercial Pd/C, Nano-Pd, $Pd(OAc)_2$ and blank cellulose catalysts to compare the activity of our C–Pd by using the model substrate of *o*-chlorotoluene. We found that the reaction did not proceed in the presence of blank cellulose, which concluded that Pd was the active center for Suzuki–Miyaura coupling reaction. The un-supported $Pd(OAc)_2$ catalyst could only yield 41.1% under the same condition, which may arise from the Pd (0) was the catalytic active center. The lower catalytic activity of commercial Pd/C with yield of 67.5% might be due to the large particle size of Pd (Fig. S3†), which resulted in the less exposed available active sites. The catalytic activity of the commercial Nano-Pd catalyst was also poor, which could attribute to the nano-Pd (Fig. S4†) were easy to agglomerate during the reaction process due to the lack of carrier.

The good catalytic activity of the C–Pd catalyst further prompted us to study its applicability in Suzuki–Miyaura coupling reaction. From Table 2, in the reaction of aryl bromide or aryl iodide and phenylboronic acid, the catalyst showed very high catalytic activity for the substrates replaced by different groups (Table 2, **3a–3i**), and the corresponding products of biaryl compounds could be obtained at very high yields (74.9–99%) and TOF values (266–2126 $h^{-1}$). As was known that, owing to the higher bond energy of C–Cl compared to the C–Br and C–I, the reaction between aryl chloride and phenylboronic acid was usually difficult to occur. Encouragingly, on the challenging reaction of aryl chloride and phenylboronic acid, the C–Pd also showed excellent catalytic activity whether the substituent groups in aryl chlorides were electron-donating or electron-withdrawing groups, with product yields of 69.4–99% and TOF values of 143–354 $h^{-1}$. It could be seen that the catalyst exhibited good substrate suitability. To compare the catalytic activity advantages of the synthesized C–Pd catalyst, we also compared the catalyst with a number of Pd-based catalysts for catalyzing the Suzuki–Miyaura coupling reaction reported in the literature. As shown in Table 3, by using the model reaction of aryl chlorides and phenylboronic acid, the C–Pd catalyst showed good catalytic activity, higher TOF values and recycle yields than most of the reported catalysts, which further proved the good catalytic performance of our catalyst. Based on the above results, the catalytic mechanism of C–Pd was illustrated in Fig. 4.[40–42] Firstly, after the addition of aryl halides, the Pd complex (Ar–Pd–X) was formed over C–Pd catalyst *via* oxidative

Table 3 Comparison of catalytic activity of some Pd-based catalysts in the Suzuki–Miyaura coupling reaction of aryl chlorobenzenes with phenylboronic acids

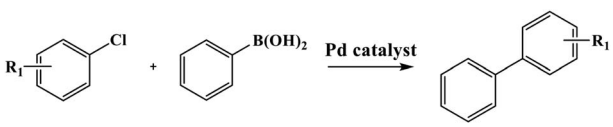


| Entry | Condition | [Pd] (mol%) | Yield (%) | TOF ($h^{-1}$) | Cycle[a] | Ref. |
|---|---|---|---|---|---|---|
| 1 | $R_1 = NO_2$, Pd–PdO/ZnO, 0.83 h, 80 °C | 3.24 | 50 | 18.6 | 5 (95%) | 43 |
| 2 | $R_1$ = Me, $Fe_3O_4$/PEG/Pd, 1 h, 60 °C | $2.2 \times 10^{-4}$ | — | — | 5 (34%) | 44 |
| 3 | $R_1 = NO_2$, $PdCl_2$, 24 h, 120 °C | 0.2 | 85 | 17.7 | 6 (90%) | 45 |
| 4 | $R_1 = NO_2$, GO-SB/Pd, 3.2 h, 100 °C | 0.8 | 59 | 23.0 | 6 (86%) | 46 |
| 5 | $R_1$ = OMe, PCIL-1, 4 h, 25 °C | 0.5 | 55 | 27.5 | 5 (91%) | 47 |
| 6 | $R_1$ = OMe, FeS@EP-AG-Pd MNPs, 12 h, 50 °C | 0.15 | 40 | 22.2 | 7 (93%) | 48 |
| 7 | $R_1 = NO_2$, PS-co-PMAA-IDA-Pd, 12 h, 80 °C | 1.0 | 68 | 5.6 | 4 (96%) | 49 |
| 8 | $R_1 = NO_2$, GO/$Fe_3O_4$/PAMPS/Pd, 24 h, 80 °C | 1 | 68 | 2.8 | 7 (92%) | 50 |
| 9 | $R_1$ = OMe, MCNTs@(A-V)-silica-Pd, 24 h, 100 °C | 1.5 | 78 | 2.2 | 7 (89%) | 51 |
| 10 | $R_1$ = OMe, $Fe_3O_4$/AO/Pd, 24 h, 25 °C | 0.1 | 60 | 25 | 7 (82%) | 52 |
| 11 | $R_1 = NO_2$, Pd-2A3HP-MCM41, 24 h, 120 °C | 0.89 | 63 | 2.9 | 8 (87%) | 53 |
| 12 | $R_1$ = OMe, Pd-NP-PIL, 4 h, 100 °C | 1.7 | 16 | 2.4 | 5 (>90%) | 54 |
| 13 | $R_1 = NO_2$, nano-Pd/$Fe_3O_4$/ZnO, 10 h, 100 °C | $9.7 \times 10^{-5}$ | 50 | 51.5 | 4 (83%) | 55 |
| 14 | $R_1 = NO_2$, Pd/FTO, 15 h, 80 °C | 0.1 | 25 | 16.7 | 5 (>90%) | 56 |
| 15 | $R_1$ = OMe, $[Al_2Pd_3(L)_6Cl_6]$, 4 h, 110 °C | 0.1 | 5 | 12.5 | 5 (94%) | 57 |
| 16 | $R_1$ = OMe, C–Pd, 6 h, 80 °C | 0.047 | >99 | 354 | 6 (>99%) | This work |

[a] The preceding number was the number of cycles, and the number in parentheses represented the yield at this number of cycles.

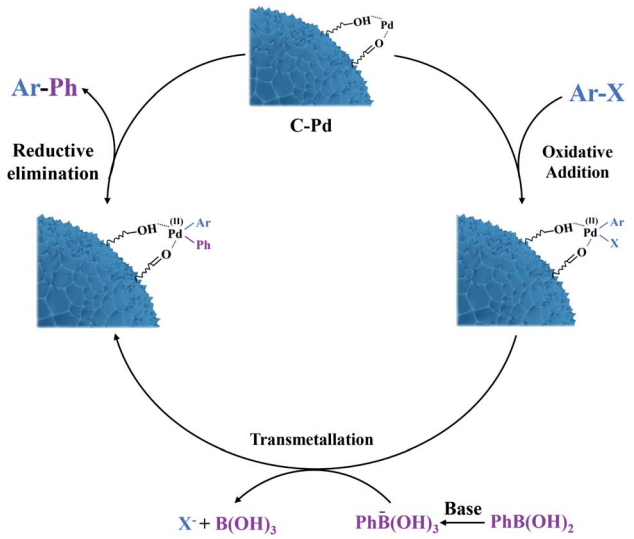


Fig. 4 The probable mechanism of the Suzuki–Miyaura coupling reaction catalyzed by C–Pd.

addition. The complex then formed an Ar–Pd–Ph complex with phenylboronic acid in the presence of $K_2CO_3$. Finally, the target compound of Ar–Ph was obtained *via* reductive elimination.

### 3.3 Catalytic recyclability of the C–Pd catalyst

Cyclic stability is also an important indicator for evaluating heterogeneous catalysts. Herein, we also conducted multiple continuous cyclic reactions based on the model reaction of *o*-chlorotoluene and phenylboronic acid. The catalyst was isolated by simple filtration in each catalytic run, as shown in Fig. 5a, the yield of the target compound was still greater than 99% after the sixth run, indicating that the catalyst had excellent reusability. XRD pattern in Fig. 5b showed that the C–Pd after six cycles still retained the peak of the blank cellulose, and the new reflection at $2\theta = 40.2$ attributed to the Pd (111).[58,59] XPS spectrum analysis was also performed on the recycled C–Pd. The full spectrum of XPS in Fig. S5† showed that the C–Pd catalyst still contained three elements of C, O and Pd, and the Pd 3d spectrum (Fig. 5c) showed that the Pd NPs in reused C–Pd was still mostly in the form of metallic Pd (0). TEM image of C–Pd after cycling was shown in Fig. 5d, which showed that the Pd NPs on the catalyst were slightly agglomerated after multiple cycles, but most Pd NPs were still uniformly dispersed on the carrier. The mean diameter of the Pd NPs in reused C–Pd was 2.80 ± 0.4 nm, which was closed to that of fresh C–Pd catalyst with 2.75 ± 0.4 nm. These results demonstrated that our catalyst showed good cycle stability in catalyzing Suzuki–Miyaura coupling reaction. The good catalytic activity and cycle stability of C–Pd could be attributed to the below reasons: (1) the nanoporous structure of cellulose microspheres could provide abundant adhesion sites for Pd particles, which was conducive to the dispersion of Pd, as well the transfer and exchange of reactants; (2) the formed tiny Pd NPs with more exposed catalytic active sites could greatly promote the catalytic reaction; (3) further, the abundant functional groups on cellulose could interact with Pd particles and fix them tightly.

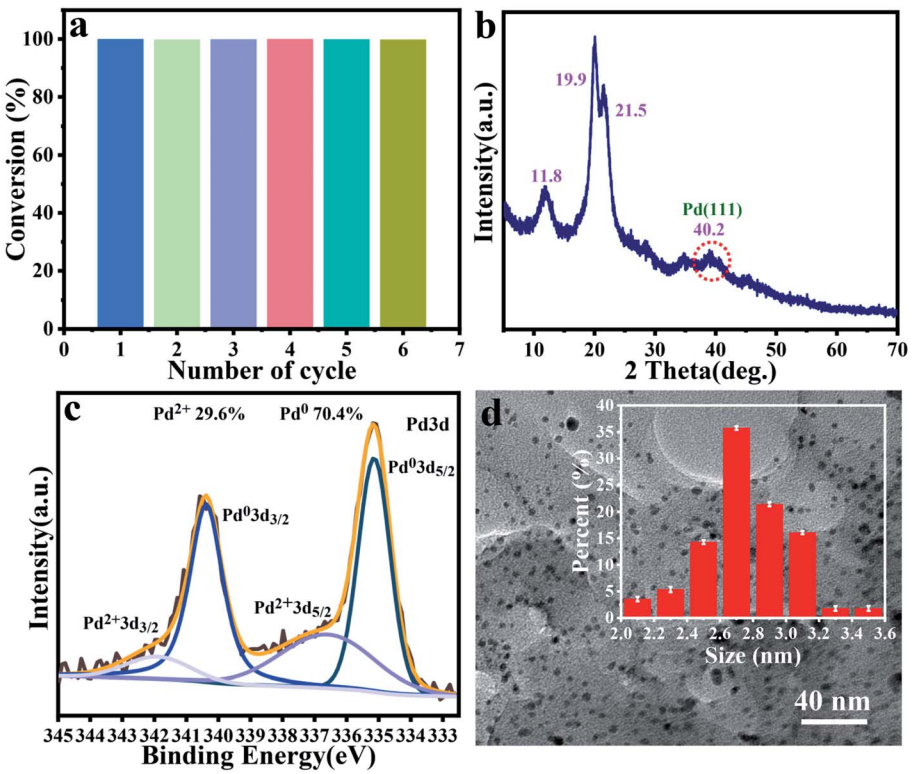


Fig. 5 Cycle activity of C–Pd in 6 runs (a). XRD pattern of C–Pd after 6 runs (b). XPS of Pd 3d spectra of C–Pd after 6 runs (c). TEM image of C–Pd after 6 runs (d).

## 4. Conclusion

In summary, an efficient Pd nano-catalyst derived from renewable biomass resource cellulose was successfully synthesized. In our discovery, the Pd NPs interacted with the hydroxyl groups on cellulose, making the active Pd sites easier to function. The nanoporous structure of cellulose also provided better conditions for the exchange and transport of substances, making it easier for catalytically active sites to function. More importantly, the supported C–Pd catalyst had excellent catalytic activity in the Suzuki–Miyaura coupling reaction, with TOF up to 2126 $h^{-1}$, as well as good recyclability with target product yield of >99% after 6 runs. We believe that the strategy proposed in this study will provide a facile and versatile method for the preparation of other biomass-based highly performance catalyst materials.

## Conflicts of interest

The authors declare that they have no known competing financial interests or personal relationships that could have appeared to influence the work reported in this paper.

## Acknowledgements

This work was supported by the Guizhou Provincial Science and Technology Foundation (No. [2020] 1Y212), the Science and Technology Top Talent Project of Guizhou Province (No. [2021] 029), the National Natural Science Foundation of China (No. 52063008), the Graduate Education Innovation Project of Guizhou Province (No. [2020] 099), the Guizhou Province Science and Technology Plan Project (No. ZK [2021] Key 050), the Guizhou Province Young Scientific and Technological Talents Growth Project (No. [2022] 172), and the Hundred Talents Project of Guizhou Province (No. [2016] 5673).

## References

1 X. F. Wan, X. Y. Wang, G. X. Chen, C. B. Guo and B. W. Zhang, *Mater. Chem. Phys.*, 2020, **246**, 122574.
2 M. H. Salehi, M. Yousefi, M. Hekmati and E. Balali, *Polyhedron*, 2019, **165**, 132–137.
3 A. Dikova, N. P. Cheval, A. Blanc, J. M. Weibel and P. Pale, *Adv. Synth. Catal.*, 2015, **357**, 4093–4100.
4 M. Kempasiddaiah, V. Kandathil, R. B. Dateer, B. S. Sasidhar, S. A. Patil and S. A. Patil, *Cellulose*, 2020, **27**, 3335–3357.
5 K. S. Bhat, V. Lanke, J. D. Prasad and K. R. Prabhu, *Appl. Catal. Gen.*, 2020, **596**, 117516.
6 P. Wang, J. Cai, J. Q. Chen and M. Ji, *J. Brazil. Chem. Soc.*, 2015, **26**, 748–754.
7 M. Pusty and P. M. Shirage, *RSC Adv.*, 2020, **10**, 10097–10112.
8 K. Dhara, B. Parasar, A. J. Patil and J. Dash, *Synth. Commun.*, 2019, **49**, 859–868.
9 T. Mondal, S. De, S. Dutta and D. Koley, *Chem.–Eur. J.*, 2018, **24**, 6155–6168.
10 H. Sharma, S. Sharma, C. Sharma, S. Paul and J. H. Clark, *Mol. Catal.*, 2019, **469**, 27–39.
11 Y. N. Chen and L. Feng, *J. Photochem. Photobiol., B*, 2020, **205**, 111807.
12 Y. S. Wu, Y. C. Zhu, J. Wang, Z. K. Shang, H. X. Jin, Y. Ding and A. G. Hu, *Chem.–Eur. J.*, 2021, 28, DOI: **10.1002/chem.202102979**.
13 N. V. Kuchkina, A. K. Haskell, S. A. Sorokina, A. S. Torozova, L. Z. Nikoshvili, E. M. Sulman, B. D. Stein, D. G. Morgan, L. M. Bronstein and Z. B. Shifrina, *ACS Appl. Mater. Interfaces*, 2020, **12**, 22170–22178.
14 H. Shen, J. Y. He, F. He, Y. R. Xue, Y. J. Li and Y. L. Li, *Appl. Catal. Gen.*, 2021, **623**, 118244.
15 R. M. Ansari and B. R. Bhat, *Chem. Phys.*, 2019, **517**, 155–160.
16 C. F. Mao, K. Yin, C. H. Yang, G. M. Dong, G. K. Tian, Y. W. Zhang and Y. M. Zhou, *J. Colloid Interface Sci.*, 2022, **608**, 809–819.
17 S. Wu, N. Ding, P. W. Jiang, L. Wu, Q. L. Feng, L. B. Zhao, Y. B. Wang, Q. Su, H. Zhang and Q. L. Yang, *Tetrahedron Lett.*, 2020, **61**, 152656.
18 K. O. Kirlikovali, Z. Chen, T. Islamoglu, J. T. Hupp and O. K. Farha, *ACS Appl. Mater. Interfaces*, 2020, **12**, 14702–14720.
19 Z. W. Kang, Z. C. Gao, S. F. Lv, F. B. Zhang and J. X. Jiang, *Silicon*, 2019, **11**, 287–292.
20 H. Yan, H. Cheng, Y. Hong, Y. Lin, T. Yao, C. Wang, J. Li, S. Wei and J. Lu, *J. Am. Chem. Soc.*, 2015, **137**, 10484.
21 N. S. Pagar, P. R. Karandikar, A. J. Chandwadkar and R. M. Deshpande, *J. Porous Mater.*, 2021, **28**, 423–433.
22 Z. Wen, Z. W. Ma, F. H. Mai, F. Yan, L. H. Yu, M. Jin, Y. S. Sang, Y. F. Bai, K. Cui, K. Wu, M. M. Chen, H. Chen and Y. D. Li, *Catal. Today*, 2020, **355**, 272–279.
23 I. Prihatiningtyas, Y. Li, Y. Hartanto, A. Vananroye, N. Coenen and B. Van der Bruggen, *Chem. Eng. J.*, 2020, **388**, 124216.
24 M. A. Hobisch, D. Muller, W. J. Fischer, A. Zankel, R. Eckhart, W. Bauer, S. Zabler and S. Spirk, *ACS Appl. Nano Mater.*, 2019, **2**, 3864–3869.
25 S. Kamel and T. A. Khattab, *Cellulose*, 2021, **28**, 4545–4574.
26 P. Singhsa, R. Narain and H. Manuspiya, *ACS Appl. Nano Mater.*, 2018, **1**, 209–221.
27 S. Li, W. P. Deng, S. S. Wang, P. Wang, D. L. An, Y. Y. Li, Q. H. Zhang and Y. Wang, *ChemSusChem*, 2018, **11**, 1995–2028.
28 A. M. Garcia, T. S. Martins and F. F. Camilo, *Cellulose*, 2021, **28**, 4899–4911.
29 D. F. Xu, X. Xiao, J. Cai, J. Zhou and L. N. Zhang, *J. Mater. Chem. A*, 2015, **3**, 16424–16429.
30 Y. Z. Li, L. Xu, B. Xu, Z. P. Mao, H. Xu, Y. Zhong, L. P. Zhang, B. J. Wang and X. F. Sui, *ACS Appl. Mater. Interfaces*, 2017, **9**, 17156–17163.
31 F. Hamano, H. Seki, M. Ke, M. Gopiraman, C. T. Lim and I. S. Kim, *Mater. Lett.*, 2016, **169**, 33–36.
32 P. Xu, C. L. Cen, N. N. Chen, H. Lin, Q. Wang, N. F. Xu, J. E. Tang and Z. G. Teng, *J. Colloid Interface Sci.*, 2018, **526**, 194–200.
33 Y. Zhang, X. Li, Y. Yang, A. Lan, X. He and M. Yu, *RSC Adv.*, 2014, **4**, 34584–34590.

34 P. S. Pharande, G. S. Rashinkar and D. M. Pore, *Res. Chem. Intermed.*, 2021, **47**, 4457–4476.
35 A. Salamatmanesh, A. Heydari and H. T. Nahzomi, *Carbohydr. Polym.*, 2020, **235**, 115947.
36 D. Paul, S. Rudra, P. Rahman, S. Khatua, M. Pradhan and P. N. Chatterjee, *J. Organomet. Chem.*, 2018, **871**, 96–102.
37 X. L. Pei, Y. Li, Y. Deng, L. J. Lu, W. D. Li, R. Y. Shi, A. W. Li and L. N. Zhang, *Carbohydr. Polym.*, 2021, **251**, 117020.
38 S. Chakraborty, M. H. Mruthunjayappa, K. Aruchamy, N. Singh, K. Prasad, D. Kalpana, D. Ghosh, N. S. Kotrappanavar and D. Mondal, *ACS Sustain. Chem. Eng.*, 2019, **7**, 14225–14235.
39 Q. Lu, Y. J. Zhang, H. Y. Hu, W. Wang, Z. Q. Huang, D. Chen, M. Yang and J. Liang, *Nanomaterials*, 2019, **9**, 275.
40 J. J. Fuentes-Rivera, M. E. Zick, M. A. Duefert and P. J. Milner, *Org. Process Res. Dev.*, 2019, **23**, 1631–1637.
41 Y. H. Wang, X. T. Qi, Q. Ma, P. Liu and G. C. Tsui, *ACS Catal.*, 2021, **11**, 4799–4809.
42 W. Shi, Y. M. Niu, S. L. Li, L. Y. Zhang, Y. Zhang, G. A. Botton, Y. Wan and B. S. Zhang, *ACS Nano*, 2021, **15**, 8621–8637.
43 F. Rezaei, R. Khalifeh and M. A. Amrollahi, *Mater. Today Chem.*, 2020, **18**, 100353.
44 A. De Cattelle, A. Billen, G. O'Rourke, W. Brullot, T. Verbiest and G. Koeckelberghs, *J. Organomet. Chem.*, 2019, **904**, 121005.
45 F. Khosravi, M. Gholinejad, D. Lledo, G. Grindlay, C. Najera and J. M. Sansano, *J. Organomet. Chem.*, 2019, **901**, 120941.
46 A. Zarnegaryan, Z. Dehbanipour and D. Elhamifar, *Polyhedron*, 2019, **170**, 530–536.
47 P. R. Boruah, P. S. Gehlot, A. Kumar and D. Sarma, *Mol. Catal.*, 2018, **461**, 54–59.
48 I. Sarvi, M. Gholizadeh and M. Izadyar, *Catal. Lett.*, 2017, **147**, 1162–1171.
49 J. Z. Zhang, J. S. Chen, Q. Y. Zhang, R. M. Wang and S. H. Wu, *Res. Chem. Intermed.*, 2019, **45**, 2503–2514.
50 S. Asadi, R. Sedghi and M. M. Heravi, *Catal. Lett.*, 2017, **147**, 2045–2056.
51 D. Khalili, A. R. Banazadeh and E. Etemadi-Davan, *Catal. Lett.*, 2017, **147**, 2674–2687.
52 R. Ghorbani-Vaghei, S. Hemmati and M. Hekmati, *J. Chem. Sci.*, 2016, **128**, 1157–1162.
53 M. Nikoorazm, A. Ghorbani-Choghamarani and M. Khanmoradi, *J. Porous Mater.*, 2016, **23**, 761–772.
54 S. Ghazali-Esfahani, E. Paunescu, M. Bagherzadeh, Z. F. Fei, G. Laurenczy and P. J. Dyson, *Sci. China Chem.*, 2016, **59**, 482–486.
55 M. Hosseini-Sarvari, A. Khanivar and F. Moeini, *J. Iran. Chem. Soc.*, 2016, **13**, 45–53.
56 S. Y. Mak, K. H. Liew, C. C. Chua, M. A. Yarmo, B. H. Yahaya, W. Z. Samad, M. S. M. Jamil and R. M. Yusop, *J. Chem. Sci.*, 2019, **131**, 111.
57 R. Wu, Y. Yao, L. Q. Wei, L. P. Li and B. H. Ye, *Inorg. Chim. Acta*, 2018, **482**, 605–611.
58 H. T. T. Vu, V. L. N. Vo and Y. M. Chung, *Appl. Catal. Gen.*, 2020, **607**, 117867.
59 S. Zhang, F. Zhang, Y. Pan, L. Jin, B. Liu, Y. Mao and J. Huang, *RSC Adv.*, 2018, **8**, 5678–5684.